chemistry

MDPI

Article

Solvatochromism and Selective Sorption of Volatile Organic Solvents in Pyridylbenzoate Metal-Organic Frameworks

Christophe A. Ndamyabera, Savannah C. Zacharias, Clive L. Oliver and Susan A. Bourne *

Centre for Supramolecular Chemistry Research, Department of Chemistry, University of Cape Town, Rondebosch 7701, South Africa

* Correspondence: susan.bourne@uct.ac.za

Received: 20 July 2019; Accepted: 13 August 2019; Published: 15 August 2019

Abstract: Using cobalt(II) as a metal centre with different solvent systems afforded the crystallization of isomorphous metal-organic frameworks $\{[Co(34pba)(44pba)]\cdot DMF\}_n$ (**1**) and $\{[Co(34pba)(44pba)]\cdot(C_3H_6O)\}_n$ (**2**) from mixed 4-(4-pyridyl)benzoate (44pba) and 3-(4-pyridyl)benzoate (34pba) ligands. Zinc(II) under the same reaction conditions that led to the formation of **1** formed an isostructural $\{[Zn(34pba)(44pba)]\cdot DMF\}_n$ framework (**3**). Crystal structures of all three MOFs were elucidated and their thermal stabilities were determined. The frameworks of **1**, **2**, and **3** were activated under vacuum to form the desolvated forms **1d**, **2d**, and **3d**, respectively. PXRD results showed that **1d** and **2d** were identical, consequently, **1d** and **3d** were then investigated for sorption of volatile organic compounds (VOCs) containing either chloro or amine moieties. Thermogravimetric analysis (TGA) and nuclear magnetic resonance (NMR) were used to determine the sorption capacity and selectivity for the VOCs. Some sorption products of **1d** with amines became amorphous, but the crystalline framework could be recovered on desorption of the amines. Investigation of the sorption of water (H_2O) and ammonia (NH_3) in **1d** gave rise to new phases identifiable by means of a colour change (solvatochromism). The kinetics of desorption of DMF, water and ammonia from frameworks **1d** and **3d** were studied using non-isothermal TGA. Activation energies for both cobalt(II) and zinc(II) frameworks are in the order $NH_3 < H_2O <$ DMF, with values for the **1d** analogue always higher than those for **3d**.

Keywords: metal-organic frameworks; vapour sorption; solvatochromism; desorption kinetics

1. Introduction

Volatile organic compounds (VOCs) are organic compounds with an appreciable vapour pressure at ambient temperature. They include naturally occurring and synthetic compounds and range in effect from harmless to toxic. Some VOCs have been shown to have malodorous, mutagenic or carcinogenic properties [1–3] and some have been implicated in causing air pollution, particularly in developing countries [4], and are partly responsible for the generation of photochemical ozone and smog precursors. They are thus considered as harmful pollutants [2,3]. Some industrial manufacturing processes, as well as the use of manufactured materials, can increase the emission of VOCs into the local environment [5,6]. As a consequence, the development of effective technologies to mitigate the emission of VOCs has received increasing attention [1]. Some reports have shown promising removal and recovery methods of VOCs from air and water through adsorption processes [7–9]. Solid adsorbents have been shown to be superior compared to other techniques of decontamination of air or water, owing to their relative low cost, wide range of applications, simplicity of design, easy operation, low harmful secondary products and the feasible regeneration of these solid adsorbents [10]. Traditional

solids adsorbents such as zeolites and activated carbon (AC) can be used for sorption purposes but they have shortcomings such as low surface area and the requirement of high temperature for their synthesis and regeneration [11,12]. Recent reports have shown that metal-organic frameworks (MOFs) have higher adsorption capacities and lower energy costs for regeneration [4,10,12].

Porous MOFs are crystalline frameworks with a wide range of possible configurations arising from the coordination of metal centres or clusters and organic linkers. MOFs can be designed to have high surface areas [10,13–15], easy functionalization, and tunable porosities, making them preferable to zeolites and activated carbon for many applications. Additionally, the coexistence of inorganic (hydrophilic) and organic (hydrophobic) moieties in MOFs structure may offer control of their interaction with guest molecules [4]. Thus, MOFs are of interest for a wide range of applications such as gas sorption [4,7,16], storage [17], separation [18–21], and sensing [22–25]. The choice of organic linker is key to MOF properties. The most commonly used linkers are those that can coordinate to metal ions via oxygen or nitrogen donors. Prior studies in our laboratories [19] and elsewhere [26] have shown that combining carboxylate and pyridyl or triazole aromatic rings allows dynamic rotation between the aromatic rings which in turn generates flexible MOFs. This is a key feature for their selective sorption capacity [19,26]. The recognition of chemical information by an adsorbent MOF may be characterised by colour change known as chromism [27,28], or reversible change in structure size known as a breathing phenomenon [19,23]. The latter has been observed in both single ligand MOFs such as $[Zn(34pba)_2]_n$ as well as in a mixed ligand MOF $[Cd(34pba)(44pba)]_n$; where the channels react to stimuli caused by the temperature and size of the entering molecules such as alkyl alcohols, N,N-dimethylformamide (DMF) and N,N-dimethylacetamide (DMA) [19,26]. However, it can be difficult to characterise the sorbed product due to a loss of crystallinity after removal or inclusion of guests [27,29–31]. Furthermore, the selective sorption capacity for VOCs such as chlorinated solvents and amines are rarely investigated. In this paper we report the synthesis of three-dimensional isomorphous and isostructural MOFs from cobalt(II) and zinc(II) with two related ligands, 3-(4-pyridylbenzoate) (34pba) and 4-(4-pyridylbenzoate) (44pba). These non-interpenetrated frameworks retain the framework structure and crystallinity on activation under vacuum. Their sorption capacity for amines and chlorinated solvents was investigated, as was their relative selectivity for sorption of chlorinated VOCs.

2. Materials and Methods

All chemicals were obtained from commercial sources and were used without further purification. $\{[Co(34pba)(44pba)]\cdot DMF\}_n$ (**1**), $\{[Co(34pba)(44pba)]\cdot(C_3H_6O)\}_n$ (**2**), and $\{[Zn(34pba)(44pba)]\cdot DMF\}_n$ (**3**) (44pba = 4-(4-pyridyl)benzoate and 34pba = 3-(4-pyridyl)benzoate) were solvothermally synthesized as detailed in Table 1. Compounds **1**, **2**, and **3** were activated at 210 °C under vacuum for 6 h which resulted in **1d**, **2d**, and **3d**, respectively. The activated samples were placed in narrow vials which were placed into larger vials containing VOCs and sealed to allow vapour sorption at room temperature (r.t., ca. 25 °C) for between one day and two weeks. The VOCs selected for study were dichloromethane (DCM), chloroform ($CHCl_3$), chlorobenzene (ClBenz), water, ammonia, methylamine ($MeNH_2$), 1-propylamine ($PropNH_2$), 1-butylamine ($ButNH_2$), benzylamine ($BzNH_2$), and 1-phenylethylamine($PhEtNH_2$). The regeneration of the activated sorbents was carried out using the same conditions as for activation.

Table 1. Experimental conditions for the synthesis of **1**, **2**, and **3**.

	Metal Salt	Ligands	Solvent System	Conditions
1	$CoCl_2\cdot 6H_2O$ (6 mg, 0.03 mmol)	34pba/44pba (10 mg, 0.050 mmol each)	DMF(6 mL)/Ethanol (2 mL)	120 °C for 3 days
2	$CoCl_2\cdot 6H_2O$ (6 mg, 0.03 mmol)	34pba/44pba (10 mg, 0.050 mmol each)	Acetonitrile(6 mL)/water (2 mL)	120 °C for 3 days
3	$Zn(NO_3)\cdot 6H_2O$ (30 mg, 0.13 mmol)	34pba/44pba (40 mg, 0.20 mmol each)	DMF(6 mL)/Ethanol (2 mL)	120 °C for 3 days

Competitive sorption for chlorinated solvents was performed by placing equivalent volumes of two different solvents into a large vial and the relevant activated MOF into a small vial. The latter was then placed into the large vial and sealed for two days for the sorption of the vapours.

2.1. Thermogravimetric Analysis (TGA) and Differential Scanning Calorimetry (DSC)

Thermogravimetric analysis (TGA) was performed using a TA Instrument TA-Q500 on 1–2 mg samples in open platinum pans under nitrogen gas flow (50 mL min^{-1}) at a heating rate of 10 °C min^{-1} within the temperature range 25–500 °C. The onset temperature for guest loss was determined using Differential scanning calorimetry (DSC). Samples of mass 1–2 mg were placed in aluminium pans with ventilated lids and heated at 10 °C min^{-1} using a TA Instrument DSC-Q200 under nitrogen gas flow (50 mL min^{-1}).

2.2. Infrared Spectroscopy

IR spectra were measured on a PerkinElmer Spectrum Two FTIR spectrometer equipped with an ATR Diamond accessory for powder samples. Samples were scanned over a range of 400–4000 cm^{-1}.

2.3. Nuclear Magnetic Resonance (NMR)

Solids containing the guest species were soaked into DMSO-d_6 and heated in order to release the guests into the solution for the NMR analysis. ^{1}H NMR spectra were recorded in DMSO-d_6 solution using a BRUKER 300 MHz spectrometer at 303 K. Appropriate signals were integrated to determine the ratio of the respective guests in the MOFs.

2.4. Powder X-ray Diffraction (PXRD)

Powder X-ray diffraction (PXRD) patterns were measured on a Bruker D8 Advance X-ray diffractometer operating in a DaVinci geometry equipped with a Lynxeye detector using CuKα-radiation (λ = 1.5406 Å). X-rays were generated at 30 kV and 40 mA. Samples were placed on a zero-background sample holder and scanned over a range of 4–40° in 2θ.

2.5. Crystal Structure Determination

Single crystals of good quality were selected using optical microscopy under plane-polarized light. Intensity data were recorded on a Bruker KAPPA APEX II DUO diffractometer using graphite monochromated Mo-Kα radiation (λ = 0.71073 Å) at 100 or 173 K. Data were corrected for Lorentz-polarization effects and for absorption (SADABS) [32]. The structures were solved by direct methods in SHELXS and refined by full-matrix least-squares on F^2 using SHELXL [33] within the XSEED [34] interface. The non-hydrogen atoms were located in difference electron density maps and were refined anisotropically while hydrogen atoms were placed in calculated positions and refined with isotropic temperature factors. Details of crystal structure refinements are given in Table 2 and Table S2.

Table 2. Crystallographic information for compounds **1**, **2**, and **3**.

Compound	1	2	3
Formula	$C_{27}H_{23}CoN_3O_5$	$C_{27}H_{22}CoN_2O_5$	$C_{27}H_{23}N_3O_5Zn$
Mass (g·mol^{-1})	528.41	513.39	534.85
Crystal size (mm^3)	0.080 × 0.10 × 0.11	0.030 × 0.060 × 0.090	0.030 × 0.030 × 0.090
Crystal system	Monoclinic	Monoclinic	Monoclinic
Space group	$P2_1/c$	$P2_1/c$	$P2_1/c$
a (Å)	9.203(2)	10.068(4)	9.339(1)
b (Å)	17.823(4)	15.632(5)	17.678(3)
c (Å)	14.718(3)	15.399(5)	14.735(2)
β (°)	92.75(3)	98.588(7)	93.189(5)
V (Å^3)	2411.3(8)	2396.4(1)	2428.84(7)
T (K)	100(2)	100(2)	173(2)
Z	4	4	4
D_c (g·cm^{-3})	1.456	1.423	1.463
μ(Mo−Kα) (mm^{-1})	0.756	0.757	1.055
F(000)	1092	1060	1104
Range scanned, θ (°)	1.80–28.34	1.87–25.09	1.80–27.58
No. reflections collected	22,928	18,219	22,013
No. unique reflection	5981	4250	5584
No. reflections with I ≥ 2σ(I)	4089	2860	3713
Parameters/restraints	327/0	318/0	327/0
Goodness of fit, S	1.034	1.024	1.006
Final R indices (I ≥ 2σ(I))	0.0859	0.0899	0.0867
Final wR2 (all data)	0.1198	0.1248	0.1107
Min, max e$^-$ density (e Å^{-3})	0.414, −0.417	0.653, −0.455	0.421, −0.443

3. Results and Discussion

The frameworks in **1**, **2**, and **3** are identical in terms of connectivity and geometry, with the asymmetric unit consisting of a metal ion (Co^{2+} in **1** and **2**, Zn^{2+} in **3**) bound to one 34pba and one 44pba linker. A centre of inversion generates a dinuclear secondary building unit (SBU) in which the two metal ions are connected by two bridging 34pba linkers through carboxylate groups while each metal ion is also coordinated to one 34pba and one 44pba through the pyridyl-N and to a 44pba through a bidentate carboxylate. The extension of this SBU through space gives rise to a double-walled network of *bcu* topology where each side of the square channels consists of a 34pba and a 44pba linker (Figure 1 and Table 2) [26]. Hour-glass shaped channels running parallel to [100] contain DMF (**1** and **3**) or acetone (**2**) guest molecules. The presence of acetone in **2** was unexpected as a mixture of acetonitrile and water had been used to prepare this compound. Conversion of acetonitrile to acetone is likely to proceed via hydrolysis to acetic acid [35] followed by ketonization to form acetone [36,37]. There are weak hydrogen bonds between the guest oxygens and the aromatic walls of the MOF. While **1** and **3** are isostructural, the structure of **2** is subtly different. Torsion angles indicate that the rings of both linkers are twisted slightly more away from coplanar in **2** than in **1** or **3**, while the orientation of the carboxylate groups is closer to coplanar with the aromatic ring in **2** than in the other compounds (see Figure S1 and Table S1 in ESI). The effect of these small changes is a lengthening of unit cell axes *a* and *c* while axis *b* shortens, but without changing the symmetry or space group. It is likely that the guest influences this change through the flexibility of the bent 34pba and linear 44pba linkers which allow a hinge-like expansion or contraction of the guest-accessible void [26].

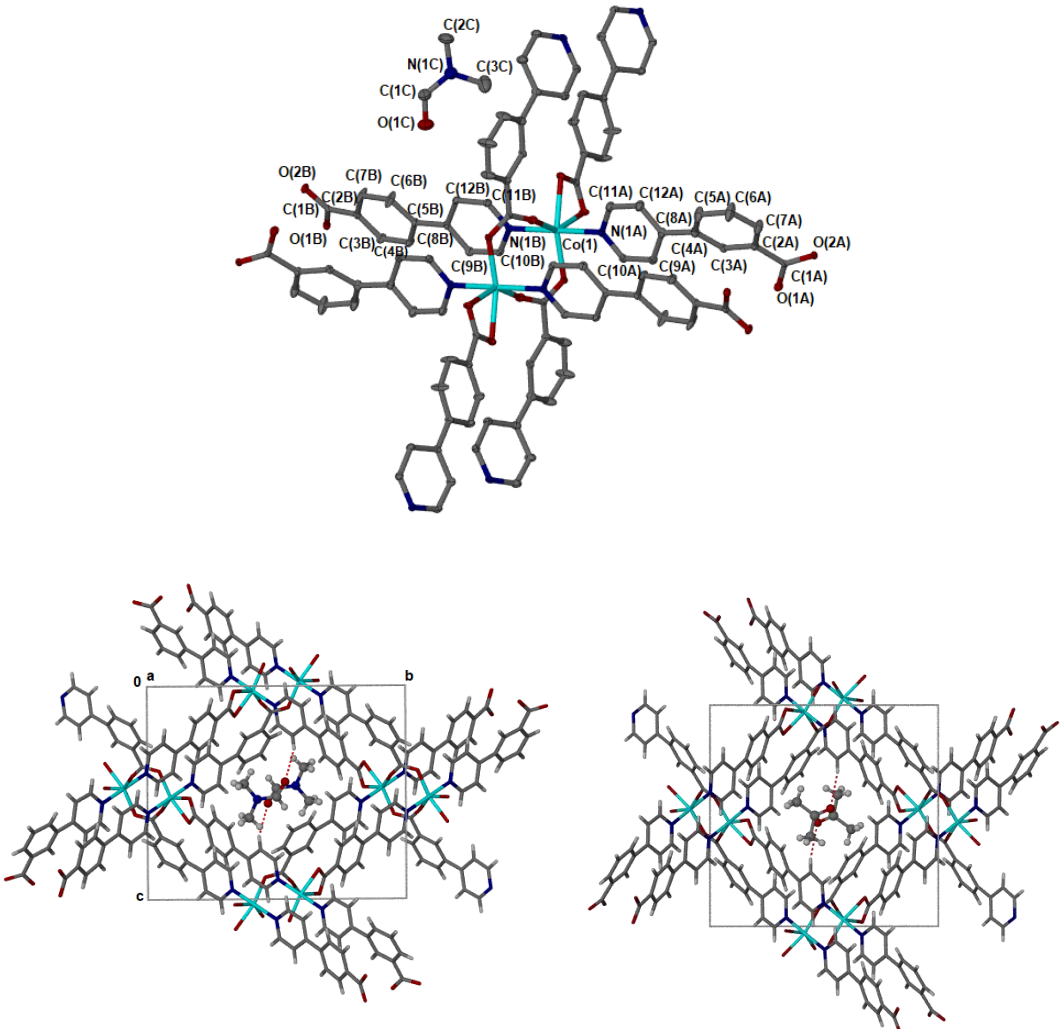

Figure 1. (**Top**) Coordination geometry and SBU in **1**. (**Bottom**) Packing diagrams of **1** (**left**) and **2** (**right**) showing the interactions between guest molecules and walls of the metal-organic frameworks (MOF).

The measured PXRD patterns in Figure 2 show the similarity of **1**, **2**, and **3** frameworks which matched well to the patterns calculated from single crystal structures. However, compound **2** had a small peak at 8.9° instead of 9.4° as for **1**. There are subtle differences in the pattern for **2** compared to those for **1** and **3**, for example, the shift in peaks at positions 12° and 21°. This dissimilarity could reflect the difference in the crystallographic data explained above. However, the activated forms of both **1d** and **2d** were the same after the removal of guest solvents. All activated forms **1d**, **2d**, and **3d** (**d**: Activated) retained their crystallinities with a slight shift of peaks (except **3d**) to higher 2θ values which corresponds to a small decrease in interplanar spacing in the frameworks after guest removal. Hence, these compounds were stable after removal of guest molecules which is not observed in all MOFs [27,29,30].

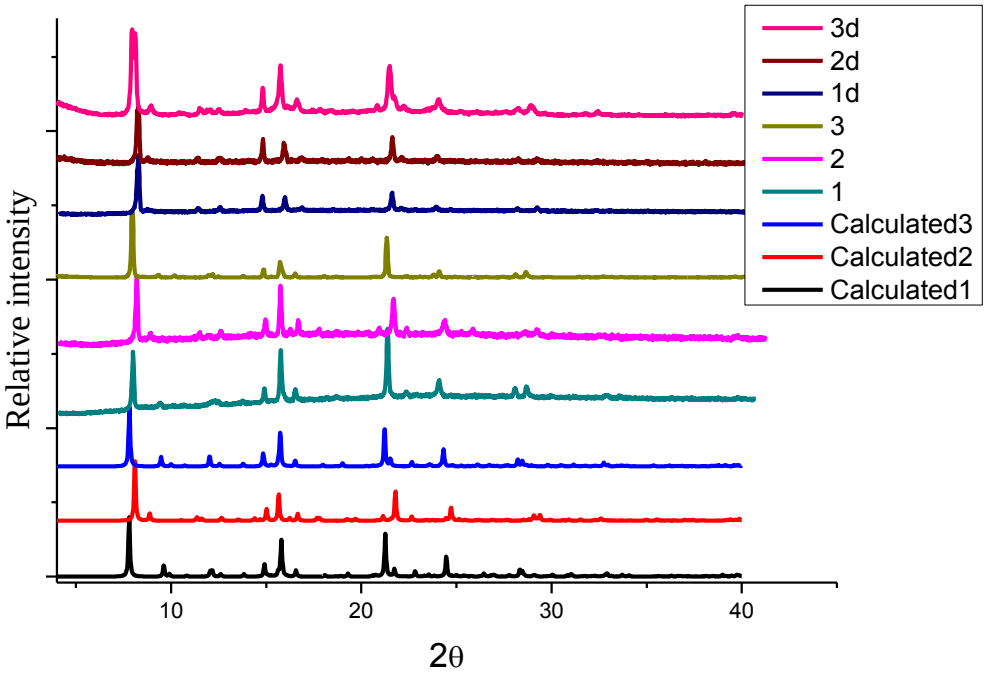

Figure 2. PXRD patterns for **1**, **2**, **3**, **1d**, **2d** and **3d** and their corresponding dry forms compared to their calculated patterns.

Carbonyl stretches in the FTIR spectra (Figure 3) confirm the presence of DMF (in **1** and **3**) at 1678 cm^{-1} and acetone (in **2**) at 1713 cm^{-1}. The removal of these guest solvents was confirmed by the absence of these bands in the spectra of **1d** and **3d**. The spectra of the activated forms were similar to one another as expected from the PXRD analysis.

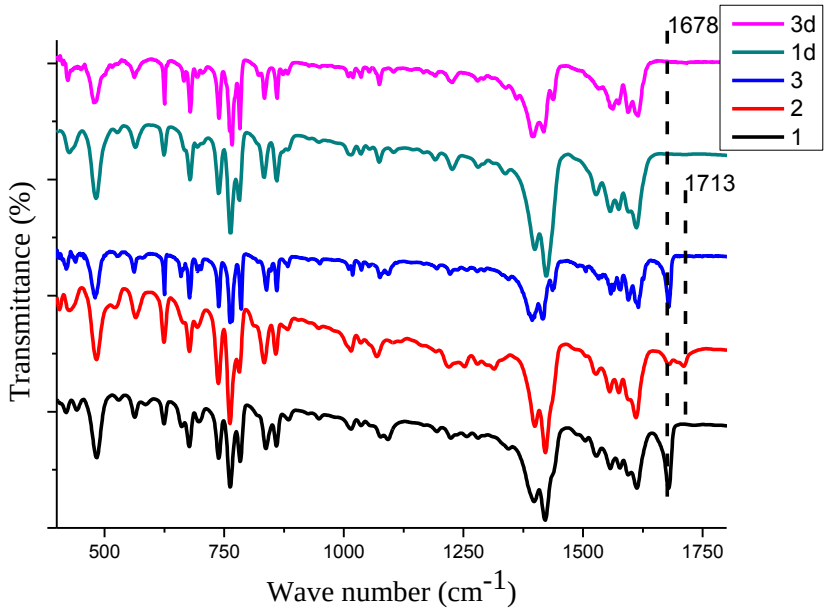

Figure 3. Infrared spectra of **1**, **2**, **3**, **1d**, and **3d** showing functional groups of guest molecules and coordination modes.

Thermogravimetric analysis (TGA) and DSC are shown in Figure 4. The weight loss of 14.1% between 120 and 216 °C in **1** was assigned to the removal of one DMF molecule (calculated 13.8%). This was characterised by a broad endothermic peak from 115–280 °C in the DSC. MOF **2** shows a total

complex weight loss of 24.5%. The corresponding DSC trace shows an endothermic peak between 110 and 150 °C, followed by a small exotherm and a broad endothermic peak between 160 and 250 °C. It is possible that the removal of the acetone guest overlaps with the decomposition of the framework. This is contradictory to the PXRD evidence that the framework is robust. It is more likely therefore that the bulk sample selected for thermal analysis may contain a mixture of crystalline forms, only some of which correspond to the MOF characterised by crystal structure elucidation. An observed weight loss of 12.7% for **3** in the range of 120 and 216 °C was attributed to the removal of one DMF molecule (calculated 13.7%). The corresponding DSC curve shows a broad endothermic process between 130 and 260 °C. The TGA traces for **1d**, **2d**, and **3d** show no mass loss before 300 °C, indicating the solvent has been removed from the framework.

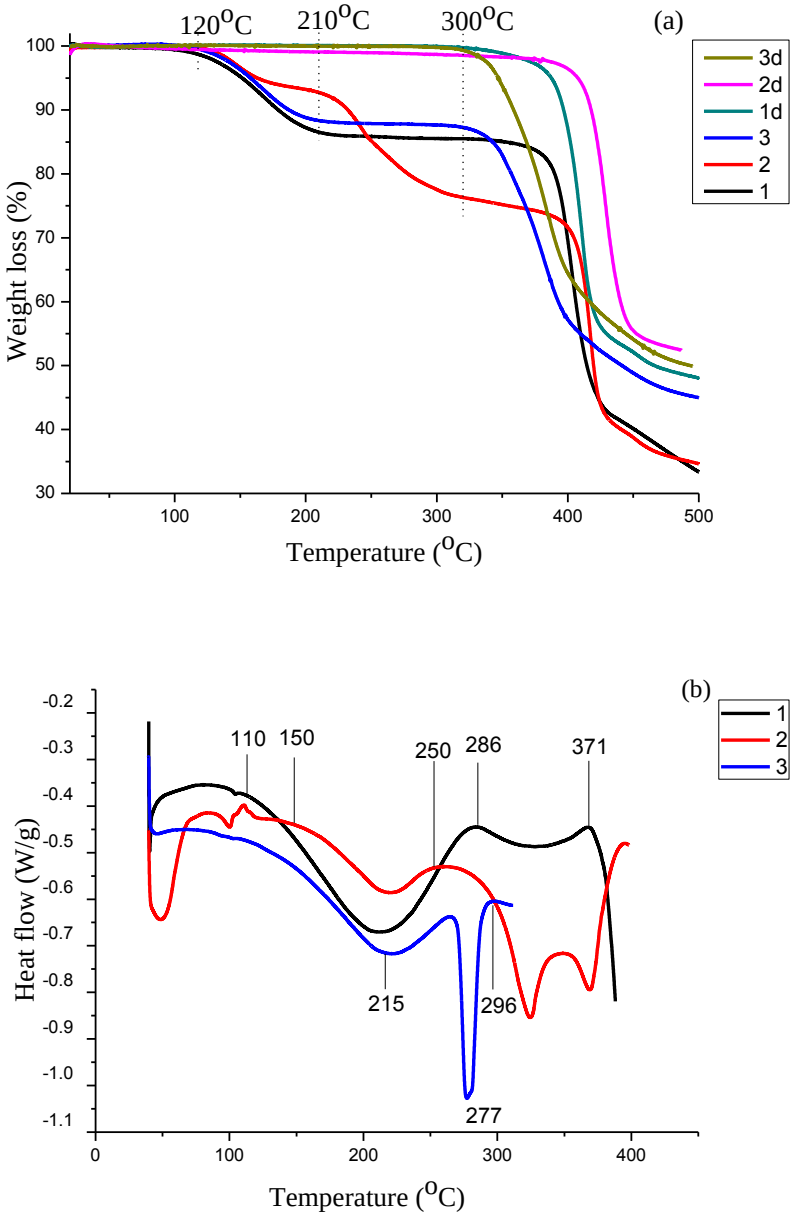

Figure 4. (**a**) TGA curves for **1**, **2**, **3**, **1d**, **2d**, and **3d** (**b**) DSC curves showing the process of the removal of guest molecules and decomposition of the framework.

3.1. Sorption of VOCs by Activated MOFs

To test the potential of these MOFs to serve as sorbents for pollutants, we carried out vapour sorption experiments using a series of chlorinated volatile organic compounds (VOCs) and another series of volatile amines. Sorption of water and of ammonia were also studied. Sorption experiments were carried out using activated samples of the Co-MOF (**1d**) and Zn-MOF (**3d**).

Sorption of chlorinated VOCs dichloromethane (DCM), chloroform ($CHCl_3$) and chlorobenzene (ClBenz) were achieved in a single crystal to single crystal manner, which allowed the elucidation of these crystal structures (Table S2 and Figure 5). The guests are stabilized in place by a number of weak interactions, including Cl···π, and C−H···π interactions and, in the case of chlorobenzene, through π···π interactions with the walls of the MOF. Comparable interactions have been observed in similar systems [38,39]. PXRD patterns (Figure S2a,b) of the phases obtained by vapour sorption of all tested chlorinated VOCs into **1d** or **3d** are unchanged from the starting activated phases, thus confirming the robustness of the retained framework structure [40].

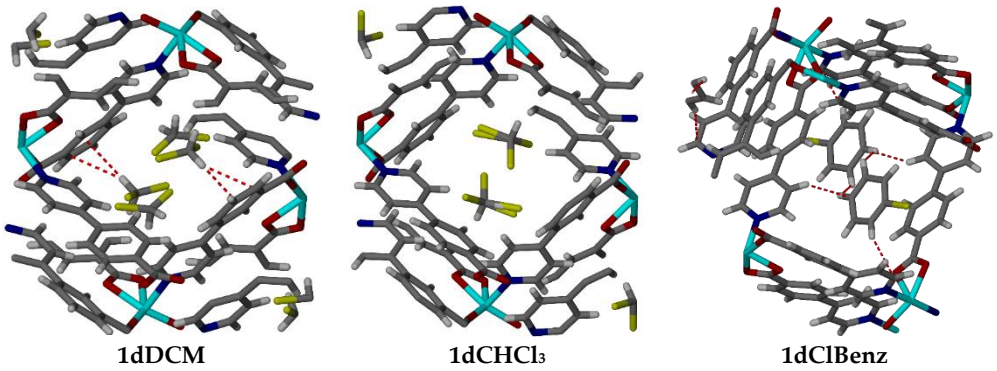

Figure 5. Inclusion of dichloromethane, chloroform and chlorobenzene into MOF **1d**.

The extent of selectivity in **1d** and **3d** was investigated from binary mixtures of the same chlorinated VOCs. Table 3 presents the solvent ratios obtained from the integration of relevant NMR peaks (Figure S5) from the competition studies. For **1d**, a mixture of DCM and chloroform were taken up without selectivity, while **3d** exposed to the same mixture selectivity absorbed DCM. Both MOFs selected DCM and chloroform over chlorobenzene from these respective binary mixtures. On the other hand, DCM was selectively sorbed 8.3 times over chlorobenzene. It should be noted that no attempt was made to compensate for differences in vapour pressure, and that the more volatile solvent was absorbed in each case, in contrast to a previous study carried out in our laboratory [19].

Table 3. Selectivity of **1d** and **3d** for chlorinated volatile organic compounds (VOCs).

1d	**Mole Ratio of VOCs in 1d** [a]	**Selectivity (Major Component)**
DCM/Chloroform	1:1	none
DCM/Chlorobenzene	8.3:1	DCM
Chloroform/Chlorobenzene	10:1	Chloroform
3d	**Mole Ratio of VOCs in 3d**	**Selectivity (Major Component)**
DCM/Chloroform	1.3:1	DCM
DCM/Chlorobenzene	1:0	DCM
Chloroform/Chlorobenzene	3:1	Chloroform

[a] Determined by NMR (Figure S5).

1d and **3d** show similar sorption trends for chlorinated VOCs as well as a series of volatile amines (Figure S3). Table 4 lists the VOC sorption results for **1d** and **3d**. PXRD traces for sorbed complexes are shown in Figure S2. The loading values were calculated from TGA analysis (Figure S4) and

compared to theoretical maximum loading capacities. The loading capacity (L_c) is calculated from the crystallographically derived void volume and the liquid density of the respective solvents. The maximum loading capacity (ML_c) for the empty networks was estimated from

$$ML_c = (\text{solvent accessible void volume})/(Z \times \text{molecular volume}). \quad (1)$$

Table 4. Uptake of selected solvents by the activated phases **1d** and **3d**.

VOC	Experimental Mass Loss, TGA (%)	Temperature Range of Mass Loss (°C)	Loading Capacity, L_c (x in Proposed Formula: {[M(34pba)(44pba)]·x Solvent}$_n$)	ML_c	% Loading Capacity
1d					
DCM	14.0	60–154	0.9	1.3	69
$CHCl_3$	17.1	118–285	0.8	1.0	80
ClBenz	13.0	87–264	0.6	0.8	75
H_2O	15.4	60–134	4.6	4.6	100
NH_3	12.9	60–150	4.0	3.5	114
$MeNH_2$	26.1	30–220	5.2	1.9	273
$PropNH_2$	33.4	30–220	3.9	1.0	390
$ButNH_2$	31.0	30–220	2.8	0.8	350
$BzNH_2$	52.0	65–260	4.6	0.8	575
$PhEtNH_2$	9.7	170–310	0.4	0.7	57
3d					
DCM	11.0	88–220	0.7	1.4	50
$CHCl_3$	13.3	110–232	0.6	1.1	55
ClBenz	11.0	61–252	0.5	0.8	63
H_2O	12.9	73–155	3.8	4.8	79
NH_3	12.5	59–127	3.9	3.6	108
$MeNH_2$	18.2	30–280	3.3	1.9	174
$PropNH_2$	18.4	30–263	1.8	1.0	180
$ButNH_2$	29.2	50–290	2.6	0.9	289
$BzNH_2$	36.0	88–290	2.4	0.8	300
$PhEtNH_2$	8.4	77–290	0.3	0.7	43

The solvent-accessible void volume of **1d** and **3d** were estimated using Mercury with a probe radius of 1.2 Å and a grid step of 0.2 Å and were found to be 549.0 and 571.4 $Å^3$ per unit cell respectively [41].

For the chlorinated solvents, the loading capacity (L_c) in the proposed formula {[M(34pba)(44pba)]·x solvent}$_n$ for both systems is lower than the maximum loading capacity. For each individual solvent, the sorption is higher for **1d** than for **3d**.

Water is taken up to near full capacity by both **1d** and **3d**, with little disruption of the framework.

To test the potential of these compounds as sorbents for amines, the activated MOFs **1d** and **3d** were exposed to the vapours of a series of amines, *viz*. ammonia (NH_3), methylamine ($MeNH_2$), propylamine ($PropNH_2$), 1-butylamine ($ButNH_2$), benzylamine ($BzNH_2$) and phenylethylamine ($PhEtNH_2$), Table 4, Figures S2 and S3. The crystal quality of the resultant compounds was too poor to allow full structural characterisation.

For all amines except phenylamine, the loading capacity of **1d** exceeds the maximum calculated from simple molecular volumes. Complexes also become amorphous. To further understand this, we exposed **1d** to benzylamine ($BzNH_2$) and found that the material remained crystalline until a mass loss of 40% was recorded. Subsequent desorption of the $BzNH_2$ from amorphous **1dBzNH$_2$** under vacuum recovered crystalline **1d** (Figure S9). In **3d** on the other hand, while the loading values obtained were again higher than the calculated maximum, the compounds retained their crystallinity but show some differences in phase in their PXRD traces. As with the chlorinated solvents, the amount sorbed by **1d** is greater than that for **3d**.

Amines are capable of hydrogen bonding, hence stronger intermolecular interactions, than chlorinated VOCs, which may allow them to pack more compactly into the channels, and to interact strongly with the internal surfaces of the MOFs, leading to higher loading values [39,42] and phase changes [43–45]. For benzylamine in particular, the MOFs took up a large amount, which could be attributed to aromatic stacking between $BzNH_2$ and the aromatic rings in the MOF walls [46]. The lower sorption capacity for $PhEtNH_2$ is the result of steric effects and lower polarity. No tests for selectivity among amine VOCs were performed.

3.2. *Solvatochromism*

Their PXRD patterns (Figure 6) show that the sorption of H_2O and NH_3 by **1d** formed new phases (**1dw** and **1dNH$_3$**, respectively) with noticeable colour changes from red to khaki (Figure 7). Upon desorption, both **1dw** and **1dNH$_3$** resulted in purple powder phases, which are amorphous (**1dwTG** and **1dNH$_3$TG**). However, the crystallinity, as well as their khaki colours, were restored after reabsorption (**1dwTGw** and **1dNH3TGNH$_3$**). Solvatochromism in MOFs has been reported to be the result of the supramolecular interactions such as hydrogen bonding and/or the coordination of the solvent molecules to the metal centres in the frameworks [27,44,47]. These interactions affect the energy associated with d-d transitions resulting in visible colour changes [27,39].

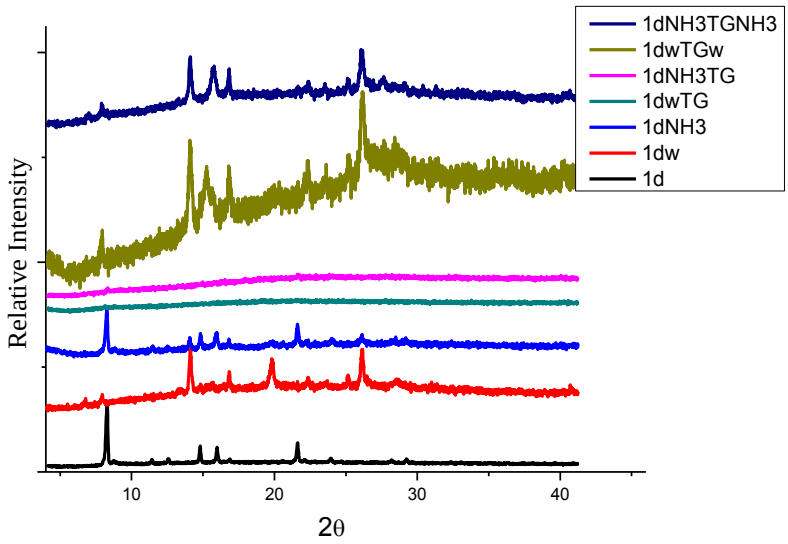

Figure 6. PXRD patterns for reversible sorption for ammonia, and H_2O by **1d**.

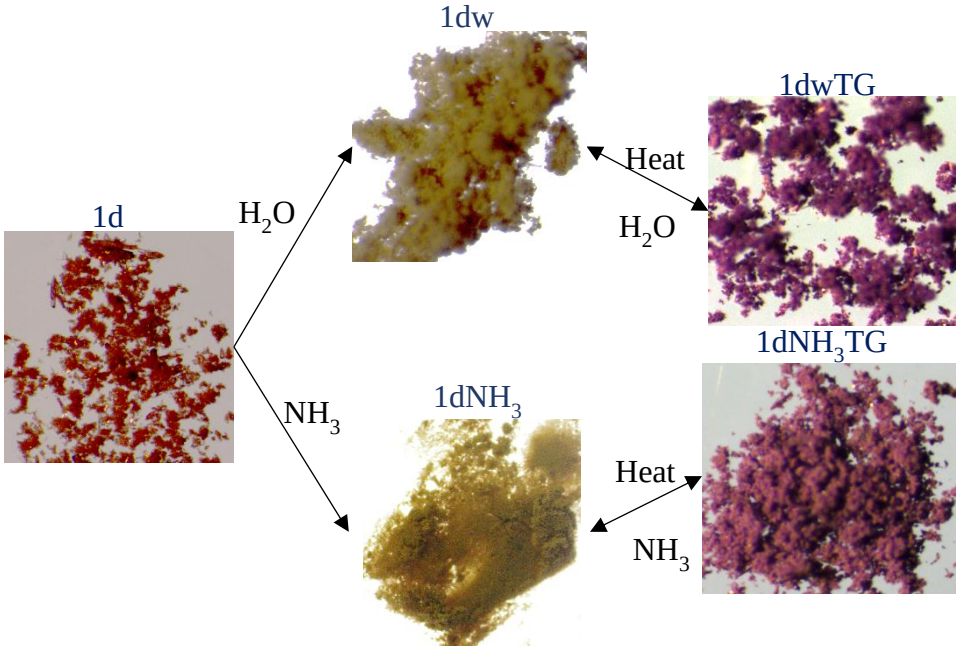

Figure 7. Reversible sorption of H_2O and NH_3 in **1d** and associated colour changes.

3.3. Kinetics of Desorption from **1** *and* **3**

TGA may be used to determine the activation energy (Ea) of the guest desorption process. We used the Ozawa model-free method [48] to study the removal of guests DMF, NH_3, and H_2O for both systems reported here. Samples of mass 1–2 mg were heated at different heating rates (5, 10, 20, and 30 °C min^{-1}) in order to determine the activation energy associated with the removal of guest molecules from **1**, **3**, **1dw**, **3dw**, **1dNH$_3$**, and **3dNH$_3$** (Figure S7). Percentage mass losses along with the corresponding temperature at each heating rate were used to determine the activation energy (E_a) according to the equation:

$$\log\beta_\alpha = \log(A_\alpha\, E_{a\alpha}/g(\alpha)R) - 2.315 - 0.457(E_{a\alpha}/RT_\alpha) \quad (2)$$

where β_α is the heating rate, A_α is the frequency factor, $E_{a\alpha}$ is the activation energy, T_α is the temperature at each conversion level, and g(α) refers to the kinetic model. Figure S8 presents the plots of $\log\beta_\alpha$ versus reciprocal absolute temperature (in the form of 1000/T K^{-1}). Equating the slope to $-0.457(E_a/RT)$ allows one to calculate the activation energies, which are given in Table 5.

Table 5. Activation energy associated with removal of guest molecules.

Mass Loss (%)	E_a (kJ mol^{-1})					
	DMF from 1d	**DMF from 3d**	**H_2O from 1dW**	**H_2O from 3dW**	**NH_3 from 1dNH$_3$**	**NH_3 from 3dNH$_3$**
20	74.77	68.77	77.3	64.78	65. 10	58.46
40	75.31	66.50	72.59	57.35	67.8	59.39
60	72.77	70.57	75.24	65.23	68.61	62.01
80	77.30	64.08	74.75	68.38	68.77	62.01
Mean	**75.04 ± 1.68**	**67.48 ± 2.81**	**74.97 ± 1.93**	**63.94 ± 4.67**	**67.57 ± 1.70**	**60.47 ± 1.82**

The activation energies determined for desorption from **1d** are higher than the corresponding desorption from **3d**. This may be attributed to the difference in the metal centre as well as the solvent-accessible volume of the channels, *viz.* 549.0 $Å^3$ in **1d** and 571.4 $Å^3$ in **3d**, as the size of the cavities influences the supramolecular interactions possible between host and guest [47,49]. Activation

energies associated with the desorption of DMF and H_2O are similar to one another but are higher than that of NH_3. Higher activation energies are generally associated with stronger host-guest interactions. The activation energies for desorption of DMF from **1d** and **3d** are comparable to those reported for the related MOF $\{[Co(34pba)_2]\cdot DMF\}_n$ [47], while the average activation energies for the desorption of H_2O for **1d** and **3d** are also comparable to those reported for $[Co(34pba)_2]$ isomers and chromium(III) terephthalate (MIL-101) [27,50]. There are no previous reports of desorption of ammonia from MOFs, so we compared our values to those reported for the desorption of NH_3 from Brønsted acid sites in zeolite ZSM-5 derivatives [51], which were found to have activation energies between 50 and 60 kJ mol^{-1}. Activation energies determined in this study are of the same order of magnitude, suggesting that intermolecular interactions such as hydrogen bonding with the channel walls are of approximately the same strength as those in the zeolite.

4. Conclusions

The coordination of two pyridylbenzoate ligands to cobalt(II) and zinc(II) metal centres formed isostructural $\{[Co(34pba)(44pba)]\cdot DMF\}_n$ (**1**) and $\{[Zn(34pba)(44pba)]\cdot DMF\}_n$ (**3**) compounds. Using an acetonitrile/water mixture instead of a DMF/ethanol solvent system led to a framework isomorphous to **1**, $\{[Co(34pba)(44pba)]\cdot(C_3H_6O)\}_n$ (**2**) where acetonitrile had undergone hydrolysis and ketonization to produce the guest acetone (C_3H_6O). These MOFs retain their phase and crystallinity (**1d** and **3d**) after the removal of guest molecules under vacuum. Both **1d** and **3d** took up chlorinated and amine VOCs and showed potential selectivity in the sorption of binary chlorinated solvent mixtures, with preference for dichloromethane and chloroform. The activated MOFs had a higher sorption capacity for amine VOCs, which was attributed to their stronger intermolecular interactions with the framework. The sorption of chlorinated VOCs did not affect the crystallinity of the frameworks while some amine VOCs led to new phases in **3d** and amorphous phases in **1d**. The crystalline phase **1d** could be recovered from these amorphous phases on desolvation under vacuum. Characteristic solvatochromism was observed in **1d** on sorption of water or ammonia. The desorption of these two guests led to a new phase, which was reversible for both colour and crystallinity. The activation energy associated with the removal of DMF, H_2O, and NH_3 from MOFs **1d** and **3d** was determined and found to be comparable with previous systems studied. This study shows the potential of the synthesised MOFs having selectivity to take up guest molecules and undergo colour changes depending on the chemical and physical properties of the guest molecules. Therefore, studies on these MOFs for sensing and separation applications are ongoing.

Supplementary Materials: Supplementary data (crystal structure data, PXRD, thermal analysis, NMR) are available online at http://www.mdpi.com/2624-8549/1/1/9/s1. Crystallographic data for this paper have been deposited with the CCDC, accession numbers 1935229-1935234. These data can be obtained free of charge via www.ccdc.cam.ac.uk/data_request/cif or by emailing data_request@ccdc.cam.ac.uk.

Author Contributions: Conceptualization S.A.B.; synthesis, crystallography, thermal analysis C.A.N.; assistance with crystallography and analysis S.C.Z. and C.L.O.; writing—original draft preparation C.A.N.; writing—review and editing S.A.B., S.C.Z. and C.L.O.; supervision S.A.B. and C.L.O.

Funding: This research was funded by the National Research Foundation of South Africa, grant number 111699.

Conflicts of Interest: The authors declare no conflict of interest. The funders had no role in the design of the study; in the collection, analyses, or interpretation of data; in the writing of the manuscript, or in the decision to publish the results.

References

1. Lewandowski, D.A. *Design of Thermal Oxidation Systems for Volatile Organic Compounds*; CRC Press LLC: Boca Raton, FL, USA, 2000.
2. Martin, L.; Ognier, S.; Gasthauer, E.; Cavadias, S.; Dresvin, S.; Amouroux, J. Destruction of Highly Diluted Volatile Organic Components (VOCs) in Air by Dielectric Barrier Discharge and Mineral Bed Adsorption. *Energy Fuels* **2008**, *22*, 576–582. [CrossRef]

3. Hinojosa-Reyes, M.; Arriaga, S.; Diaz-Torres, L.A.; Rodríguez-González, V. Gas-Phase Photocatalytic Decomposition of Ethylbenzene over Perlite Granules Coated with Indium Doped TiO_2. *Chem. Eng. J.* **2013**, *224*, 106–113. [CrossRef]
4. Zhao, Z.; Wang, S.; Yang, Y.; Li, X.; Li, J.; Li, Z. Competitive Adsorption and Selectivity of Benzene and Water Vapor on the Microporous Metal Organic Frameworks (HKUST-1). *Chem. Eng. J.* **2015**, *259*, 79–89. [CrossRef]
5. Braek, A.M.; Almehaideb, R.A.; Darwish, N.; Hughes, R. Optimization of Process Parameters for Glycol Unit to Mitigate the Emission of BTEX/VOCs. *Process Saf. Environ. Prot.* **2001**, *79*, 218–232. [CrossRef]
6. Lee, Y.K.; Kim, H.J. The Effect of Temperature on VOCs and Carbonyl Compounds Emission from Wooden Flooring by Thermal Extractor Test Method. *Build. Environ.* **2012**, *53*, 95–99. [CrossRef]
7. Yang, K.; Sun, Q.; Xue, F.; Lin, D. Adsorption of Volatile Organic Compounds by Metal–Organic Frameworks MIL-101: Influence of Molecular Size and Shape. *J. Hazard. Mater.* **2011**, *195*, 124–131. [CrossRef] [PubMed]
8. Long, C.; Li, Q.; Li, Y.; Liu, Y.; Li, A.; Zhang, Q. Adsorption Characteristics of Benzene-Chlorobenzene Vapor on Hypercrosslinked Polystyrene Adsorbent and a Pilot-Scale Application Study. *Chem. Eng. J.* **2010**, *160*, 723–728. [CrossRef]
9. Bacchi, A.; Bourne, S.; Cantoni, G.; Cavallone, S.A.M.; Mazza, S.; Mehlana, G.; Pelagatti, P.; Righi, L. Reversible Guest Removal and Selective Guest Exchange with a Covalent Dinuclear Wheel-and-Axle Metallorganic Host Constituted by Half-Sandwich Ru(II) Wheels Connected by a Linear Diphosphine Axle. *Cryst. Growth Des.* **2015**, *15*, 1876–1888. [CrossRef]
10. Khan, N.A.; Hasan, Z.; Jhung, S.H. Adsorptive Removal of Hazardous Materials Using Metal-Organic Frameworks (MOFs): A Review. *J. Hazard. Mater.* **2013**, *244–245*, 444–456. [CrossRef]
11. Zhou, L.; Chen, Y.; Zhang, X.; Tian, F.; Zu, Z. Zeolites Developed from Mixed Alkali Modified Coal Fly Ash for Adsorption of Volatile Organic Compounds. *Mater. Lett.* **2014**, *119*, 140–142. [CrossRef]
12. Jhung, S.H.; Lee, J.H.; Yoon, J.W.; Serre, C.; Férey, G.; Chang, J.S. Microwave Synthesis of Chromium Terephthalate MIL-101 and Its Benzene Sorption Ability. *Adv. Mater.* **2007**, *19*, 121–124. [CrossRef]
13. Kobalz, M.; Lincke, J.; Kobalz, K.; Erhart, O.; Bergmann, J.; Lässig, D.; Lange, M.; Möllmer, J.; Gläser, R.; Staudt, R.; et al. Paddle Wheel Based Triazolyl Isophthalate MOFs: Impact of Linker Modification on Crystal Structure and Gas Sorption Properties. *Inorg. Chem.* **2016**, *55*, 3030–3039. [CrossRef] [PubMed]
14. Lincke, J.; Lässig, D.; Kobalz, M.; Bergmann, J.; Handke, M.; Möllmer, J.; Lange, M.; Roth, C.; Möller, A.; Staudt, R.; et al. An Isomorphous Series of Cubic, Copper-Based Triazolyl Isophthalate MOFs: Linker Substitution and Adsorption Properties. *Inorg. Chem.* **2012**, *51*, 7579–7586. [CrossRef] [PubMed]
15. Llewellyn, P.L.; Bourrelly, S.; Serre, C.; Vimont, A.; Daturi, M.; Hamon, L.; De Weireld, G.; Chang, J.-S.; Hong, D.-Y.; Hwang, Y.K.; et al. High Uptakes of CO2 and CH4 in Mesoporous Metal–Organic Frameworks MIL-100 and MIL-101. *Langmuir* **2008**, *24*, 7245–7250. [CrossRef] [PubMed]
16. Junghans, U.; Kobalz, M.; Erhart, O.; Preißler, H.; Lincke, J.; Möllmer, J.; Krautscheid, H.; Gläser, R. A Series of Robust Copper-Based Triazolyl Isophthalate Mofs: Impact of Linker Functionalization on Gas Sorption and Catalytic Activity. *Materials (Basel)* **2017**, *10*, 338. [CrossRef] [PubMed]
17. Xiang, Z.; Hu, Z.; Yang, W.; Cao, D. Lithium Doping on Metal-Organic Frameworks for Enhancing H2 Storage. *Int. J. Hydrogen Energy* **2012**, *37*, 946–950. [CrossRef]
18. Lv, X.; Shi, L.; Li, K.; Li, B.; Li, H. An Unusual Porous Cationic Metal – Organic Framework Fast and Highly Efficient Dichromate Trapping through a Single-Crystal to Single-Crystal Process. *Chem. Commun.* **2017**, *53*, 1860–1863. [CrossRef] [PubMed]
19. Mehlana, G.; Bourne, S.; Ramon, G. The Role of C–H$\cdots\pi$ Interactions in Modulating the Breathing Amplitude of a 2D Square Lattice Net: Alcohol Sorption Studies. *CrystEngComm* **2014**, *16*, 8160. [CrossRef]
20. Bhadra, B.N.; Ahmed, I.; Jhung, S.H. Remarkable Adsorbent for Phenol Removal from Fuel: Functionalized Metal–Organic Framework. *Fuel* **2016**, *174*, 43–48. [CrossRef]
21. Zhang, X.; Zhang, Y.Z.; Zhang, D.S.; Zhu, B.; Li, J.R. A Hydrothermally Stable Zn(II)-Based Metal-Organic Framework: Structural Modulation and Gas Adsorption. *Dalton Trans.* **2015**, *44*, 15697–15702. [CrossRef] [PubMed]
22. Tang, Y.-Y.; Wang, C.-J.; Chen, S.; Dai, H.-Y. A Terbium(III) Organic Framework as a Fluorescent Probe for Selectively Sensing of Organic Small Molecules and Metal Ions Especially Nitrobenzene and Fe^{3+}. *J. Coord. Chem.* **2017**, *70*, 3996–4007. [CrossRef]
23. Mahata, P.; Mondal, S.K.; Singha, D.K.; Majee, P. Luminescent Rare-Earth-Based MOFs as Optical Sensors. *Dalton Trans.* **2017**, *46*, 301–328. [CrossRef] [PubMed]

24. Wu, Y.; Yang, G.-P.; Zhao, Y.; Wu, W.-P.; Liu, B.; Wang, Y.-Y. Three New Solvent-Directed Cd(II)-Based MOFs with Unique Luminescent Properties and Highly Selective Sensors for Cu(2+) Cations and Nitrobenzene. *Dalton Trans.* **2015**, *44*, 3271–3277. [CrossRef] [PubMed]
25. Hulanicki, A.; Glab, S.; Ingman, F. Chemical Sensors Definitions and Classification. *Int. Union Pure Appl. Chem.* **1991**, *63*, 1247–1250. [CrossRef]
26. Zhou, H.L.; Zhang, Y.B.; Zhang, J.P.; Chen, X.M. Supramolecular-Jack-like Guest in Ultramicroporous Crystal for Exceptional Thermal Expansion Behaviour. *Nat. Commun.* **2015**, *6*, 1–7. [CrossRef] [PubMed]
27. Dzesse T, C.N.; Nfor, E.N.; Bourne, S.A. Vapor Sorption and Solvatochromism in a Metal-Organic Framework of an Asymmetric Pyridylcarboxylate. *Cryst. Growth Des.* **2018**, *18*, 416–423. [CrossRef]
28. Mehlana, G.; Ramon, G.; Bourne, S.A. Methanol Mediated Crystal Transformations in a Solvatochromic Metal Organic Framework Constructed from Co(II) and 4-(4-Pyridyl) Benzoate. *CrystEngComm* **2013**, *15*, 9521–9529. [CrossRef]
29. Davies, K.; Bourne, S.A.; Öhrström, L.; Oliver, C.L. Anionic Zinc-Trimesic Acid MOFs with Unusual Topologies: Reversible Hydration Studies. *Dalton Trans.* **2010**, *39*, 2869–2874. [CrossRef]
30. Lässig, D.; Lincke, J.; Moellmer, J.; Reichenbach, C.; Moeller, A.; Gläser, R.; Kalies, G.; Cychosz, K.A.; Thommes, M.; Staudt, R.; et al. A Microporous Copper Metal-Organic Framework with High H^2 and CO_2 Adsorption Capacity at Ambient Pressure. *Angew. Chem. Int. Ed.* **2011**, *50*, 10344–10348. [CrossRef]
31. Kubo, M.; Ushiyama, H.; Shimojima, A.; Okubo, T. Investigation on Specific Adsorption of Hydrogen on Lithium-Doped Mesoporous Silica. *Adsorption* **2011**, *17*, 211–218. [CrossRef]
32. Sheldrick, G.M. *SADABS, Version 2.05*; University of Göttingen: Göttingen, Germany, 2007.
33. Sheldrick, G.M. A short history of SHELX. *Acta Crystallogr. A* **2008**, *64*, 112–122. [CrossRef] [PubMed]
34. Barbour, L.J. X-Seed—A software tool for supramolecular crystallography. *J. Supramol. Chem.* **2001**, *1*, 189–191. [CrossRef]
35. Wang, Z.; Richter, S.M.; Rozema, M.J.; Schellinger, A.; Smith, K.; Napolitano, J.G. Potential Safety Hazards Associated with Using Acetonitrile and a Strong Aqueous Base. *Org. Process Res. Dev.* **2017**, *21*, 1501–1508. [CrossRef]
36. Bennett, J.A.; Parlett, C.M.A.; Isaacs, M.A.; Durndell, L.J.; Olivi, L.; Lee, A.F.; Wilson, K. Acetic Acid Ketonization over Fe_3O_4/SiO_2 for Pyrolysis Bio-Oil Upgrading. *ChemCatChem* **2017**, *9*, 1648–1654. [CrossRef] [PubMed]
37. Lukevics, E.; Stonkus, V.; Liepina, I.; Edolfa, K.; Jansone, D.; Leite, L.; Lukevics, E. Theoretical Study of the Ketonization Reaction Mechanism of Acetic Acid. *Latvian J. Chem.* **2009**, *1*, 61–67.
38. Mehlana, G.; Bourne, S.A.; Ramon, G. A New Class of Thermo- and Solvatochromic Metal–Organic Frameworks Based on 4-(Pyridin-4-Yl)Benzoic Acid. *Dalton Trans.* **2012**, *41*, 4224. [CrossRef] [PubMed]
39. Hu, Z.; Deibert, B.J.; Li, J. Luminescent Metal–Organic Frameworks for Chemical Sensing and Explosive Detection. *Chem. Soc. Rev.* **2014**, *43*, 5815–5840. [CrossRef] [PubMed]
40. Gao, Q.; Xu, J.; Cao, D.; Chang, Z.; Bu, X.H. A Rigid Nested Metal–Organic Framework Featuring a Thermoresponsive Gating Effect Dominated by Counterions. *Angew. Chem. Int. Ed.* **2016**, *55*, 15027–15030. [CrossRef]
41. Macrae, C.F.; Bruno, I.J.; Chisholm, J.A.; Edgington, P.R.; Mccabe, P.; Pidcock, E.; Rodriguez-monge, L.; Taylor, R.; Van De Streek, J.; Wood, P.A. Mercury CSD 2.0—New Features for the Visualization and Investigation of Crystal Structures. *J. Appl. Crystallogr.* **2008**, *41*, 466–470. [CrossRef]
42. Hwang, Y.K.; Hong, D.Y.; Chang, J.S.; Jhung, S.H.; Seo, Y.K.; Kim, J.; Vimont, A.; Daturi, M.; Serre, C.; Férey, G. Amine Grafting on Coordinatively Unsaturated Metal Centers of MOFs: Consequences for Catalysis and Metal Encapsulation. *Angew. Chem. Int. Ed.* **2008**, *47*, 4144–4148. [CrossRef] [PubMed]
43. Prodi, L.; Bolletta, F.; Montalti, M.; Zaccheroni, N. Luminescent Chemosensors for Transition Metal Ions. *Coord. Chem. Rev.* **2000**, *205*, 59–83. [CrossRef]
44. Britt, D.; Tranchemontagne, D.; Yaghi, O.M. Metal-Organic Frameworks with High Capacity and Selectivity for Harmful Gases. *Proc. Natl. Acad. Sci. USA* **2008**, *105*, 11623–11627. [CrossRef] [PubMed]
45. Dybtsev, D.N.; Chun, H.; Kim, K. Rigid and Flexible: A Highly Porous Metal–Organic Framework with Unusual Guest-Dependent Dynamic Behavior. *Angew. Chem. Int. Ed.* **2004**, *116*, 5143–5146. [CrossRef]
46. Kim, H.; Kim, S.; Kim, J.; Ahn, W. Liquid Phase Adsorption of Selected Chloroaromatic Compounds over Metal Organic Frameworks. *Mater. Res. Bull.* **2013**, *48*, 4499–4505. [CrossRef]

47. Mehlana, G.; Bourne, S.A.; Ramon, G.; Öhrström, L. Concomitant Metal Organic Frameworks of Cobalt(II) and 3-(4-Pyridyl) Benzoate: Optimized Synthetic Conditions of Solvatochromic and Thermochromic Systems. *Cryst. Growth Des.* **2013**, *13*, 633–644. [CrossRef]
48. Ozawa, T. A New Method of Analyzing Thermogravimetric Data. *Bull. Chem. Soc. Jpn.* **1965**, *38*, 1881–1886. [CrossRef]
49. Khuong, T.; Ramsahye, N.A.; Trens, P.; Tanchoux, N.; Serre, C.; Fajula, F.; Férey, G. Microporous and Mesoporous Materials Adsorption of C5–C9 Hydrocarbons in Microporous MOFs MIL-100 (Cr) and MIL-101 (Cr): A Manometric Study. *Microporous Mesoporous Mater.* **2010**, *134*, 134–140.
50. Xian, S.; Yu, Y.; Xiao, J.; Zhang, Z.; Xia, Q.; Wang, H.; Li, Z. RSC Advances Competitive Adsorption of Water Vapor with VOCs Dichloroethane, Ethyl Acetate and Benzene on MIL-101(Cr) in Humid Atmosphere. *RSC Adv.* **2015**, *5*, 1827–1834. [CrossRef]
51. Costa, C.; Dzikh, I.P.; Lopes, M.; Lemos, F. Activity–Acidity Relationship in Zeolite ZSM-5. Application of Bronsted-Type Equations. *Mol. Catal. A* **2000**, *154*, 193–201. [CrossRef]